Research Square

Preprints are preliminary reports that have not undergone peer review.
They should not be considered conclusive, used to inform clinical practice,
or referenced by the media as validated information.

Inflammatory CAF-derived PTGDS promotes T-cell infiltration and restrains pancreatic cancer through PGD2–DP2–NF-κB/CCL2 signaling

Yangcheng Liu
Fourth Military Medical University
Yifan Ma
Fourth Military Medical University
Yifan Guo
Fourth Military Medical University
Dengxu Tan
Fourth Military Medical University
Hongping Luo
Fourth Military Medical University
Wenlan Zhang
Fourth Military Medical University
Caiqin Zhang
Fourth Military Medical University
Changhong Shi
changhong@fmmu.edu.cn
Fourth Military Medical University

Research Article

Keywords:

Posted Date: November 24th, 2026

DOI: https://doi.org/10.21203/rs.3.rs-11696670/v1

License: This work is licensed under a Creative Commons Attribution 4.0 International License.
Read Full License

Additional Declarations: No competing interests reported.

Inflammatory CAF-derived PTGDS promotes T-cell infiltration and restrains pancreatic cancer through PGD2–DP2–NF-κB/CCL2 signaling

Yangcheng Liu[1,2 †], Yifan Ma[1,2 †], Yifan Guo[1,2 †], Dengxu Tan [1,2], Hongping Luo[1,3], Wenlan Zhang[1,3], Caiqin Zhang[1,2], Changhong Shi[1,2*]

1, Division of Cancer Biology, Laboratory Animal Center, Fourth Military Medical University, Xi'an, Shaanxi 710032, China

2, State Key Laboratory of Holistic Integrative Management of Gastrointestinal Cancers, Xi'an, Shaanxi 710032, China.

3, Gansu University of Chinese Medicine, Lanzhou 730030, China

*Correspondence:

Changhong Shi, Division of Cancer Biology, Laboratory Animal Center, The Fourth Military Medical University, Xi'an, Shaanxi 710032, China, Tel: 86-29-84774787, Fax: 86-29-83242045, Email: changhong@fmmu.edu.cn.

Abstract

Cancer-associated fibroblasts (CAFs) are major determinants of immune exclusion in pancreatic ductal adenocarcinoma (PDAC), yet the molecular programs through which distinct fibroblast states regulate T-cell accessibility remain poorly understood. Here, we identify prostaglandin D2 synthase (PTGDS) as a unique immune-regulatory program enriched in inflammatory CAFs (iCAFs) that correlates with elevated $CD8^+$ T-cell infiltration and improved clinical outcomes in PDAC. Functionally, increasing PTGDS expression in CAFs elevated prostaglandin D2 (PGD2) production, promoted intratumoral $CD8^+$ T-cell accumulation, and restrained pancreatic tumor growth. Exogenous PGD2 treatment recapitulated these effects and enhanced the antitumor activity of PD-1 blockade. Mechanistically, PGD2 signaled through its receptor DP2 to suppress NF-κB activation and CCL2 production in CAFs. In vivo, CCL2 restoration reversed both tumor growth restraint and the T-cell-permissive phenotype conferred by PTGDS-expressing CAFs. These findings establish CCL2 as a functional

downstream mediator of the PTGDS–PGD2 pathway and define a stromal PTGDS–PGD2–DP2–NF-κB/CCL2 axis linking fibroblast lipid metabolism to immune accessibility in PDAC.

Highlights

PTGDS marks an iCAF program associated with a T-cell-infiltrated PDAC state.

CAF-derived PGD2 signals through DP2 to suppress NF-κB–CCL2 signaling.

PTGDS/PGD2 restrains PDAC and enhances the antitumor activity of PD-1 blockade.

Introduction

Pancreatic ductal adenocarcinoma (PDAC) remains one of the most lethal malignancies, with limited therapeutic options and a persistently poor prognosis. Surgical resection offers the only potential for cure, yet most patients present with unresectable or metastatic disease, for which cytotoxic chemotherapy remains the mainstay of systemic treatment [1-3]. In contrast to its efficacy in several other solid tumors, immune checkpoint blockade (ICB) has shown little activity in unselected PDAC[4-6]. In a randomized phase II trial of previously treated metastatic PDAC, durvalumab monotherapy produced no objective responses, whereas combined durvalumab and tremelimumab achieved an objective response rate of only 3.1% [4]. Clinical responses remain largely confined to the uncommon subset of tumors with mismatch repair deficiency or microsatellite instability[7]. This resistance is closely associated with the distinctive PDAC microenvironment, in which a dense fibroinflammatory stroma, abundant myeloid populations, and limited accumulation of functional cytotoxic T cells collectively constrain antitumor immunity[3,6,8]. Defining the stromal programs that maintain this immune-refractory state is therefore important for extending the benefit of immunotherapy in PDAC.

Cancer-associated fibroblasts (CAFs) constitute a major component of the PDAC stroma, but their functions are heterogeneous and context dependent[8-10]. Broad depletion of fibroblasts or suppression of desmoplasia can accelerate pancreatic tumor

progression in experimental models, indicating that stromal fibroblasts are not uniformly tumor promoting[11,12]. Subsequent single-cell studies have resolved multiple CAF states, including myofibroblastic CAFs (myCAFs), inflammatory CAFs (iCAFs), and antigen-presenting CAFs (apCAFs)[12,13]. iCAFs are distinguished by secretory and inflammatory transcriptional programs, whereas myCAFs preferentially express contractile and extracellular matrix-associated genes; these states are dynamically regulated by microenvironmental signals, including opposing IL-1/JAK–STAT and TGF-β pathways[14]. Such heterogeneity raises the possibility that specific fibroblast programs may either reinforce or alleviate immune exclusion[14,15]. However, the molecular determinants that confer these divergent immunological properties remain incompletely understood.

Lipid mediators represent one potential mechanism through which fibroblasts communicate with neighboring immune cells[16,17]. Prostaglandin D2 synthase (PTGDS), also known as lipocalin-type prostaglandin D synthase, catalyzes the conversion of the cyclooxygenase-derived intermediate PGH2 to prostaglandin D2 (PGD2), thereby linking arachidonic acid metabolism to extracellular lipid signaling[18]. PGD2 can signal through the G-protein-coupled receptors DP1 (PTGDR) and DP2 (PTGDR2/CRTH2), whose downstream effects vary substantially across cellular contexts[18,19]. Although PGD2 signaling has established roles in inflammatory and immune regulation[19-21], its function within the pancreatic tumor stroma remains poorly understood. In particular, whether PTGDS defines a functionally distinct CAF state and whether fibroblast-derived PGD2 regulates antitumor immunity in PDAC have not been established.

The chemokine network represents a potential downstream interface linking stromal lipid signaling to tumor immunity. CAFs serve as major sources of cytokines and chemokines that govern the recruitment and spatial organization of immune cell populations within tumors[22-24]. CCL2, a principal ligand for CCR2, promotes the recruitment of inflammatory monocytes and the accumulation of immunosuppressive myeloid populations in pancreatic cancer[25,26]. Elevated tumoral CCL2, together with

low $CD8^+$ T-cell infiltration, correlates with worse survival[27], whereas disruption of CCR2-dependent monocyte recruitment enhances antitumor immunity in experimental models[25,27]. CCL2 expression is also tightly coupled to inflammatory transcriptional programs controlled by NF-κB[14,28], raising the possibility that metabolic signals from CAFs could alter immune-cell recruitment by modulating NF-κB-dependent chemokine production. Here, we identify PTGDS as a feature of iCAFs associated with a T-cell-infiltrated PDAC microenvironment. We show that CAF-derived PTGDS increases PGD2 production and promotes antitumor immunity through a DP2-dependent suppression of NF-κB–CCL2 signaling. CCL2 reconstitution abrogates the tumor-suppressive and T-cell-permissive phenotypes of PTGDS-expressing CAFs, while PGD2 enhances the antitumor activity of PD-1 blockade. These findings define a fibroblast lipid–chemokine circuit that regulates immune accessibility in PDAC.

Materials and Methods

Human specimens and bioinformatic analyses

Human pancreatic ductal adenocarcinoma (PDAC) specimens were obtained from patients who underwent surgical resection at Xijing Hospital, Fourth Military Medical University. The study was approved by the Medical Ethics Committee of Xijing Hospital, Fourth Military Medical University (approval no. KY20253502-1).

Bulk RNA-sequencing data and corresponding clinical information for PDAC were obtained from The Cancer Genome Atlas pancreatic adenocarcinoma cohort (TCGA-PAAD). Gene expression values were converted to transcripts per million (TPM) and log2(TPM + 1)-transformed. Kaplan–Meier survival analysis was performed after stratification according to PTGDS expression. Immune-cell infiltration was estimated using CIBERSORT with the LM22 signature matrix, and correlations between PTGDS expression and immune-cell abundance were evaluated by Spearman correlation. Pathway enrichment analysis was performed for PTGDS-associated genes.

Single-cell RNA-sequencing datasets GSE231535 and GSE154778 were obtained

from the Gene Expression Omnibus and analyzed using a standard Seurat workflow, including quality control, normalization, data integration, dimensionality reduction, clustering, and UMAP visualization. Major cell populations were annotated according to established lineage markers. CAFs were further reclustered into apCAFs, $CTGF^+$ CAFs, ECM-CAFs, iCAFs, $MMP11^+$ CAFs, myCAFs, and proliferating CAFs according to their transcriptional characteristics. Cell–cell communication between CAFs and T cells was inferred using CellChat, and metabolic pathway activity was evaluated using scMetabolism.

Primary cell isolation, culture, and PTGDS overexpression

Primary KPC tumor cells and CAFs were established from spontaneous pancreatic tumors arising in KPC (*LSL-Kras$^{G12D/+}$; LSL-$^{Trp53R172H/+}$; Pdx1-Cre*) mice. Fresh tumor tissues were washed with ice-cold PBS containing antibiotics (Servicebio, G0002), and necrotic regions were removed. Tumors were minced into approximately 1-mm^3 fragments and subjected to explant culture. After attachment, tissue fragments were maintained at 37°C with 5% CO_2 until fibroblast-like cells migrated from the explants. CAFs were maintained in DMEM/F12 (Servicebio, G4612) supplemented with 10% fetal bovine serum (Gibco, 10100147) and penicillin–streptomycin (Solarbio, P1400). Primary KPC tumor cells were maintained in DMEM (Gibco, C11995500BT) supplemented with 10% fetal bovine serum. CAF identity was confirmed by morphology and immunofluorescence staining for FAP (Affinity, AF5344) and α-SMA (Servicebio, GB13044).

For PTGDS overexpression, CAFs at approximately 50–60% confluence were transduced with PTGDS-expressing or control lentivirus in the presence of Polybrene (10 μg/mL; Hanheng Biotechnology, HB-PB-500). After 6 h, the medium was replaced with fresh complete medium. Forty-eight hours later, cells were selected with puromycin (2–5 μg/mL; Servicebio, G4017) for 5–7 days. PTGDS overexpression was confirmed by qRT-PCR and immunoblotting before subsequent experiments.

$CD8^+$ T-cell isolation, coculture, and flow cytometry

Splenocytes were isolated from C57BL/6J mice by mechanical dissociation through 70-μm cell strainers, followed by erythrocyte lysis using ACK lysis buffer (Beyotime, C3702). $CD8^+$ T cells were purified using a mouse $CD8^+$ T-cell magnetic isolation kit (Beaver, 70902-100) and activated with anti-CD3 (2 μg/mL; Thermo Fisher Scientific, 16-0031-81) and anti-CD28 (2 μg/mL; Thermo Fisher Scientific, 16-0281-81) for 24 h. Activated $CD8^+$ T cells were cocultured with control or PTGDS-overexpressing CAFs using 0.4-μm Transwell inserts for 48 h. T cells were subsequently collected and stained with anti-mouse CD25 antibody (Thermo Fisher Scientific, 12-0251-82) for 30 min at 4°C. Flow-cytometric data were acquired using a BD flow cytometer and analyzed with FlowJo v10.8.1. CD25 expression within the magnetically purified $CD8^+$ T-cell population was used to assess T-cell activation.

Animal models and in vivo treatments

Female KPC and C57BL/6J mice, 6–8 weeks of age, were obtained from GemPharmatech Co., Ltd. (Jiangsu, China) and maintained under specific pathogen-free conditions at the Laboratory Animal Center of Fourth Military Medical University. All animal experiments were approved by the Institutional Animal Care and Use Committee of Fourth Military Medical University (approval no. IACUC-20231209).

For the CAF–tumor cell coimplantation model, control or PTGDS-overexpressing CAFs were mixed with KPC tumor cells at a 4:1 ratio, and a total of 1×10^6 cells were implanted subcutaneously into C57BL/6J mice. When tumors reached approximately 50–100 mm^3, mice were randomly assigned to the NC, OE, NC + anti-PD-1, or OE + anti-PD-1 groups (n = 6 per group). Anti-PD-1 antibody (Bio X Cell, BE0146) was administered intraperitoneally at 10 mg/kg every 3 days.

To evaluate the effects of exogenous PGD2, subcutaneous tumors were established in C57BL/6J mice using tumor tissues derived from spontaneous KPC pancreatic tumors. Mice were assigned to vehicle, PGD2, anti-PD-1, or PGD2 plus anti-PD-1 groups (n = 6 per group). PGD2 (MedChemExpress, HY-101988) was administered intraperitoneally at 1 mg/kg once daily, and anti-PD-1 antibody was administered

intraperitoneally at 10 mg/kg every 3 days.

For CCL2 rescue experiments, control or PTGDS-overexpressing CAFs were mixed with KPC tumor cells at a 4:1 ratio and implanted subcutaneously into C57BL/6J mice. Mice were assigned to NC, OE, or OE + CCL2 groups (n = 6 per group). Beginning on day 6 after implantation, recombinant mouse CCL2 (MedChemExpress, HY-P7764) was administered intratumorally at 5 μg/kg once daily.

Tumor dimensions were measured every 3 days, and tumor volume was calculated as 0.5 × length × width². At the experimental endpoint, tumors were excised, weighed, and processed for subsequent histological analyses.

Patient-derived organoid–PhCAF–PBMC coculture and viability assay

Patient-derived organoids (PDOs) were established from freshly resected human PDAC tissues and maintained in organoid culture medium (HYK2101; Bozhen Biotechnology, China). Primary human pancreatic cancer-associated fibroblasts (PhCAFs) were isolated from the corresponding fresh tumor tissues and used within five passages. PDOs, PhCAFs, and peripheral blood mononuclear cells (PBMCs) used in each experiment were obtained from the same patient to establish a fully autologous coculture system.

PBMCs were activated with anti-CD3 (2 μg/mL) and anti-CD28 (2 μg/mL) for 24 h before coculture. PDOs together with control or PTGDS-overexpressing PhCAFs were placed in the lower chamber of the Transwell system, whereas activated autologous PBMCs were added to the upper chamber at 2 × 10^6 cells per well. For rescue experiments, recombinant human CCL2 was added at a final concentration of 100 ng/mL.

At the experimental endpoint, cells from the PDO-containing compartment were enzymatically dissociated into single-cell suspensions. EpCAM-positive tumor epithelial cells were enriched using human EpCAM (CD326) MicroBeads (Miltenyi Biotec, 130-061-101). Viability of the enriched tumor epithelial cells was quantified using the CellTiter-Glo 3D Cell Viability Assay (Promega, G9681), and luminescence

was measured using a BioTek microplate reader and normalized to the corresponding control group.

RNA sequencing, qRT-PCR, and ELISA

For transcriptomic analysis, primary CAFs were treated with vehicle or PGD2 (10 μM) for 48 h. Total RNA was collected and submitted to a commercial sequencing provider for library preparation and high-throughput RNA sequencing. Differentially expressed genes were subjected to KEGG pathway enrichment, gene set enrichment analysis (GSEA), and protein–protein interaction analysis.

For qRT-PCR, total RNA was extracted using a total RNA extraction kit (Tiangen, DP419). One microgram of RNA was reverse-transcribed using PrimeScript RT Master Mix (TaKaRa, RR036A), and quantitative PCR was performed using TB Green Premix (TaKaRa, RR820A). Relative gene expression was calculated using the $2^{-\Delta\Delta Ct}$ method with Actb as the reference gene.

PGD2 concentrations in CAF-conditioned medium and cell lysates were measured using a PGD2 ELISA kit (Elabscience, E-EL-0066). CCL2 concentrations in CAF-conditioned medium were determined using a mouse CCL2 ELISA kit (Thermo Fisher Scientific, 88-7391-88). Samples were collected after the indicated treatments, clarified by centrifugation, and analyzed according to the manufacturers' instructions.

Immunoblotting and pharmacological treatments

Cells were lysed in RIPA buffer supplemented with protease and phosphatase inhibitors, and protein concentrations were determined using a BCA assay. Equal amounts of protein were separated by SDS-PAGE and transferred onto PVDF membranes. After blocking, membranes were incubated with primary antibodies overnight at 4°C, followed by HRP-conjugated secondary antibodies. Protein bands were visualized using enhanced chemiluminescence and quantified using ImageJ. Primary antibodies included PTGDS (MedChemExpress, HY-P81994), phospho-p65 (Abcam, ab86299), total p65 (Cell Signaling Technology, 8242S), and GAPDH (Engibody, AT0010).

To examine NF-κB-dependent regulation of CCL2, CAFs were treated with PGD2 (10 μM; MedChemExpress, HY-101988), BAY 11-7082 (5 μM; MedChemExpress, HY-13453), or LPS (1 μg/mL; MedChemExpress, HY-D1056), alone or in the indicated combinations. BAY 11-7082 was added 1 h before subsequent stimulation where applicable. To determine the PGD2 receptor responsible for this effect, CAFs were pretreated for 1 h with the DP1 antagonist asapiprant (1 μM; MedChemExpress, HY-16763) or the DP2 antagonist AZD1981 (1 μM; MedChemExpress, HY-15950), followed by PGD2 treatment. CCL2 mRNA expression was assessed by qRT-PCR, CCL2 secretion by ELISA, and NF-κB activation by immunoblotting for phosphorylated and total p65.

Histology, immunohistochemistry, and immunofluorescence

Tumor tissues were fixed in 4% paraformaldehyde (Servicebio, G1101), paraffin-embedded, sectioned, and processed for hematoxylin and eosin staining, immunohistochemistry, or immunofluorescence. For immunohistochemistry, deparaffinized sections underwent heat-mediated antigen retrieval followed by incubation with primary antibodies overnight at 4°C. Signals were visualized using HRP/DAB detection and counterstained with hematoxylin. Primary antibodies included PTGDS (MedChemExpress, HY-P81994), Ki-67 (Abcam, ab16667), CD8 (Servicebio, GB15068), GZMB (Abcam, ab255598), and PD-L1 (Proteintech, 66248-1-Ig).

For immunofluorescence, cultured cells or tissue sections were incubated with the indicated primary antibodies followed by appropriate fluorophore-conjugated secondary antibodies and DAPI nuclear counterstaining. Antibodies used included FAP (Affinity, AF5344), α-SMA (Servicebio, GB13044), PTGDS, CD8, and CCL2 (Abcam, ab308522). Images used for quantitative comparisons were acquired under comparable imaging conditions, and staining was quantified using ImageJ.

Statistical analysis

Statistical analyses were performed using GraphPad Prism 9.0.0 and R. Data are presented as mean ± standard deviation (SD) unless otherwise indicated.

Comparisons between two independent groups were performed using an unpaired two-tailed Student's *t* test. Comparisons among three or more groups were performed using one-way ANOVA followed by Tukey's multiple-comparisons test. Longitudinal tumor-growth curves were analyzed using two-way repeated-measures ANOVA followed by Sidak's multiple-comparisons test. Kaplan–Meier survival curves were compared using the log-rank test. Spearman correlation was used to assess associations between PTGDS expression and immune-cell abundance, whereas Pearson correlation was used for the association between PTGDS expression and the composite T-cell transcriptional score. All statistical tests were two-sided, and $P < 0.05$ was considered statistically significant.

Results

PTGDS is preferentially expressed in inflammatory CAFs and is associated with favorable clinical outcome in PDAC

We first examined the expression and clinical relevance of PTGDS in PDAC. Analysis of bulk transcriptomic data showed that PTGDS expression was significantly lower in pancreatic tumors than in normal pancreatic tissues (Fig. 1A). Despite its reduced expression in tumors, higher PTGDS expression was associated with prolonged overall survival (Fig. 1B), suggesting that PTGDS expression may define a clinically favorable tumor state.

To determine the cellular source of PTGDS within the PDAC microenvironment, we integrated single-cell RNA-sequencing datasets GSE231535 and GSE154778 and resolved the major malignant, stromal, and immune cell populations (Fig. 1C). Mapping PTGDS expression across these populations revealed a marked enrichment in CAFs, with comparatively little expression in malignant epithelial cells or other major cell types (Fig. 1D, E). These data identified CAFs as the predominant PTGDS-expressing population within the PDAC microenvironment.

We next asked whether PTGDS expression was associated with a specific fibroblast

state. Reclustering of the CAF compartment resolved seven transcriptionally distinct populations, including antigen-presenting CAFs (apCAFs), $CTGF^+$ CAFs, extracellular matrix CAFs (ECM-CAFs), inflammatory CAFs (iCAFs), $MMP11^+$ CAFs, myofibroblastic CAFs (myCAFs), and proliferating CAFs (prolif-CAFs) (Fig. 1F, G). PTGDS expression was highly heterogeneous across these populations and was most prominent in iCAFs (Fig. 1H, I), identifying PTGDS as a feature of the inflammatory CAF state.

We further examined the cellular localization of PTGDS in human PDAC specimens. Immunofluorescence staining demonstrated substantial PTGDS expression within FAP-positive stromal cells, supporting its localization to the fibroblast compartment in human tumors (Fig. 1J). Collectively, these findings identify inflammatory CAFs as a major cellular source of PTGDS in PDAC and establish an association between elevated PTGDS expression and favorable clinical outcome.

PTGDS expression is associated with a T-cell-infiltrated tumor microenvironment in PDAC

Given the association between PTGDS expression and favorable clinical outcome, we next asked whether PTGDS was linked to the immune landscape of PDAC. KEGG analysis of PTGDS-associated genes revealed enrichment of several immune-related pathways, including T-cell receptor and chemokine signaling (Fig. 2A). Consistent with this observation, immune deconvolution analysis showed that PTGDS expression was positively associated with multiple lymphoid populations, including $CD8^+$ T cells (Fig. 2B). These findings suggested that elevated PTGDS expression accompanies a more immune-infiltrated tumor state.

Because our single-cell analysis identified CAFs as the predominant source of PTGDS, we next examined their relationship with T cells within the tumor ecosystem. Ligand–receptor inference revealed extensive predicted communication between fibroblast populations and T cells (Fig. 2C). At the bulk transcriptomic level, PTGDS expression

was positively correlated with a composite T-cell transcriptional score (Pearson $r = 0.72$, $P = 0.0013$; Fig. 2D), further associating PTGDS with increased T-cell representation in PDAC.

We then examined whether this relationship was evident in human PDAC tissues. Immunohistochemical analysis showed sparse $CD8^+$ T-cell infiltration in tumors with low stromal PTGDS expression, whereas tumors with higher PTGDS expression exhibited more prominent $CD8^+$ T-cell infiltration (Fig. 2E). Together, these findings consistently associate stromal PTGDS expression with a T-cell-infiltrated tumor microenvironment, raising the possibility that PTGDS-expressing CAFs participate in regulating immune-cell recruitment in PDAC.

CAF-derived PTGDS restrains pancreatic tumor growth and enhances responsiveness to PD-1 blockade

To establish an experimentally tractable system for investigating the functional role of CAF-derived PTGDS, we isolated primary fibroblasts from spontaneous pancreatic tumors arising in KPC mice. Tumor formation was confirmed by ultrasonography and histopathological examination (Supplementary Fig. S1A–C). Primary CAFs were subsequently isolated from KPC tumors by serial adherence and expansion (Supplementary Fig. S1D), and their fibroblast identity was confirmed by FAP immunofluorescence staining (Supplementary Fig. S1E).

We next generated KPC-derived CAFs with enforced PTGDS expression, which was confirmed by immunoblotting (Supplementary Fig. S1F). As an initial assessment of whether fibroblast PTGDS could influence T-cell responses, we established a CAF–T-cell coculture system (Supplementary Fig. S1G). T cells cocultured with PTGDS-overexpressing CAFs exhibited an increased proportion of $CD25^+$ cells compared with those cocultured with control CAFs (Supplementary Fig. S1H), suggesting that elevated PTGDS expression in CAFs can modulate T-cell activation status.

We then asked whether increasing PTGDS expression specifically in CAFs was

sufficient to alter pancreatic tumor growth and the response to immune checkpoint blockade in vivo. KPC tumor cells were admixed with either control or PTGDS-overexpressing KPC-derived CAFs and subcutaneously implanted into immunocompetent C57BL/6J mice, followed by treatment with anti-PD-1 or the corresponding control (Fig. 3A). Tumors containing PTGDS-overexpressing CAFs grew substantially more slowly than those containing control CAFs, resulting in reduced tumor volume and tumor weight at endpoint (Fig. 3B–D). Anti-PD-1 treatment further suppressed tumor growth, with the greatest tumor inhibition observed in mice bearing tumors containing PTGDS-overexpressing CAFs and receiving anti-PD-1 treatment (Fig. 3B–D). These findings indicate that increasing PTGDS expression within the fibroblast compartment is sufficient to restrain pancreatic tumor growth and is associated with enhanced antitumor activity of PD-1 blockade.

We next examined whether these effects were accompanied by remodeling of the tumor immune microenvironment. Immunohistochemical analysis showed reduced Ki-67 staining in tumors containing PTGDS-overexpressing CAFs, consistent with decreased tumor proliferative activity (Fig. 3E, F). In parallel, PTGDS overexpression in CAFs increased intratumoral $CD8^+$ T-cell accumulation and GZMB expression, and both were further increased in combination with anti-PD-1 treatment (Fig. 3E, F). Conversely, PD-L1 staining was reduced in tumors containing PTGDS-overexpressing CAFs and was lowest in the combination group (Fig. 3E, F).

Together, these findings establish a functional link between CAF-derived PTGDS and antitumor immunity. The initial coculture experiments suggest that PTGDS-expressing CAFs can alter T-cell activation status, while the in vivo studies demonstrate that increasing PTGDS expression in the fibroblast compartment restrains pancreatic tumor growth and is accompanied by increased $CD8^+$ T-cell accumulation and effector activity. The enhanced antitumor activity observed when PTGDS-overexpressing CAFs were combined with PD-1 blockade further supports the concept that stromal PTGDS promotes a tumor microenvironment more permissive to checkpoint

immunotherapy.

PGD2 mediates the tumor-restraining and immunomodulatory effects of CAF-derived PTGDS

Given that PTGDS catalyzes the conversion of PGH2 to PGD2, we next sought to determine whether PGD2 mediates the tumor-suppressive phenotype associated with PTGDS-expressing CAFs. Analysis of PGD2-associated metabolic transcriptional activity showed higher scores in PTGDS-high than in PTGDS-low cells (Fig. 4A), linking elevated PTGDS expression to an enhanced PGD2-related metabolic state. Consistent with this association, PTGDS overexpression in KPC-derived CAFs significantly increased PGD2 levels both in the culture supernatant and intracellular compartment (Fig. 4B, C).

We further investigated whether PGD2 was sufficient to reproduce the antitumor effects of CAF-derived PTGDS in vivo. Administration of PGD2 markedly suppressed tumor growth and reduced endpoint tumor weight, while combined PGD2 and anti-PD-1 treatment produced the greatest tumor inhibition among the treatment groups (Fig. 4D–G). Histological analysis further showed reduced Ki-67 staining and increased $CD8^+$ T-cell infiltration and GZMB expression following PGD2 treatment, changes that were further accentuated in the combination group (Fig. 4H). PD-L1 staining was concurrently reduced. Thus, exogenous PGD2 recapitulated the tumor-suppressive and immune-infiltrating phenotype observed in PTGDS-overexpressing CAFs and enhanced the antitumor efficacy of PD-1 blockade.

PGD2 suppresses CCL2 expression in CAFs

To define the molecular program through which PGD2 remodels the immune-regulatory properties of CAFs, we performed transcriptomic profiling of CAFs following PGD2 treatment. KEGG analysis of differentially expressed genes identified cytokine–cytokine receptor interaction among the most significantly enriched pathways, together

with alterations in inflammatory signaling pathways including TNF and NF-κB signaling (Fig. 5A). Consistently, GSEA revealed significant enrichment of the cytokine–cytokine receptor interaction gene set among PGD2-responsive transcripts (Fig. 5B). These findings pointed to cytokine and chemokine regulation as a prominent component of the CAF response to PGD2.

We next interrogated the PGD2-responsive network to identify candidate mediators of this transcriptional response. Protein–protein interaction analysis placed CCL2 among the highly connected nodes within the network (Fig. 5C). We therefore examined a panel of CAF-derived cytokines and chemokines by qPCR. Among all tested genes, CCL2 exhibited the most pronounced reduction following PGD2 treatment, whereas most other candidates were unchanged or showed comparatively modest changes (Fig. 5D). Consistent with the transcriptional response, CCL2 concentration in CAF-conditioned medium was significantly reduced by PGD2 treatment (Fig. 5E).

We further examined CCL2 expression in tumors from the in vivo PGD2 treatment experiment. Immunofluorescence staining demonstrated that PGD2 treatment markedly reduced intratumoral CCL2 abundance in pancreatic tumors (Fig. 5F, G). Collectively, these data identify CCL2 suppression as a prominent component of the CAF transcriptional response to PGD2 and provide a candidate chemokine mechanism linking PGD2 signaling to remodeling of the tumor immune microenvironment.

CCL2 suppression mediates the tumor-restraining and T-cell-permissive effects of CAF-derived PTGDS

We next sought to determine whether CCL2 suppression is functionally required for the antitumor effects mediated by CAF-derived PTGDS. KPC tumor cells were co-implanted with control or PTGDS-overexpressing CAFs into C57BL/6J mice, followed by CCL2 administration to restore CCL2 signaling in tumors containing PTGDS-overexpressing CAFs (Fig. 6A). Consistent with our previous findings, PTGDS

overexpression in CAFs markedly suppressed tumor growth and reduced endpoint tumor weight. CCL2 supplementation reversed this phenotype, restoring tumor growth despite sustained PTGDS overexpression in CAFs (Fig. 6B–D).

To examine whether this reversal was accompanied by alterations in T-cell infiltration, we analyzed tumor tissues. Tumors bearing PTGDS-overexpressing CAFs exhibited reduced CCL2 abundance alongside increased $CD8^+$ T-cell infiltration. In contrast, CCL2 supplementation restored intratumoral CCL2 levels and markedly diminished $CD8^+$ T-cell accumulation (Fig. 6E–G). These rescue experiments place CCL2 downstream of stromal PTGDS and support CCL2 suppression as a functional determinant of the T-cell-permissive phenotype associated with PTGDS-expressing CAFs.

To determine whether this regulatory relationship was conserved in human PDAC, we established a fully patient-matched coculture system comprising patient-derived PDAC organoids, primary PhCAFs, and activated autologous PBMCs (Fig. 6H). PTGDS overexpression in PhCAFs reduced the viability of EpCAM-positive tumor epithelial cells in the presence of activated autologous PBMCs, whereas CCL2 supplementation substantially restored tumor-cell viability (Fig. 6I, J). These findings extend the PTGDS–CCL2 regulatory relationship to a patient-derived human system and support CCL2 suppression as a functional component of the enhanced antitumor immune response associated with PTGDS-expressing CAFs.

PGD2 suppresses NF-κB–CCL2 signaling in CAFs through DP2

To determine how PGD2 represses CCL2 expression in CAFs, we further interrogated the transcriptomic profiles of PGD2-treated CAFs. GSEA revealed significant alterations in the NF-κB signaling pathway (Fig. 7A). Given the central role of p65/RELA in NF-κB-dependent inflammatory transcription, we next examined p65 activation following PGD2 treatment. PGD2 markedly reduced p65 phosphorylation without substantially altering total p65 abundance (Fig. 7B), indicating suppression of

NF-κB activation rather than changes in p65 expression.

We next asked whether NF-κB activity was functionally linked to CCL2 regulation. Pharmacological inhibition of NF-κB with BAY 11-7082 reduced p65 phosphorylation, whereas LPS robustly increased p65 activation. Notably, PGD2 attenuated the LPS-induced increase in p-p65 (Fig. 7C). These changes were accompanied by corresponding alterations in CCL2 expression and secretion: BAY 11-7082 reduced CCL2, LPS increased CCL2, and PGD2 counteracted the LPS-induced increase in CCL2 (Fig. 7D, E). Together, these findings indicate that suppression of NF-κB signaling contributes to PGD2-mediated repression of CCL2 in CAFs.

Because PGD2 can signal through both DP1 and DP2 receptors, we next sought to determine which receptor mediated this response in CAFs. Pharmacological blockade of DP2 with AZD1981 substantially reversed the PGD2-induced reduction in p65 phosphorylation, whereas blockade of DP1 with asapiprant had little effect on the suppressive action of PGD2 (Fig. 7F). Consistently, AZD1981, but not asapiprant, restored CCL2 expression and secretion toward control levels in PGD2-treated CAFs (Fig. 7G, H). These receptor-discrimination experiments support a DP2-dependent mechanism linking PGD2 to suppression of NF-κB–CCL2 signaling in CAFs.

Together with the functional rescue by CCL2, these findings delineate a PTGDS–PGD2–DP2–NF-κB/CCL2 signaling axis through which CAFs regulate the immune microenvironment of PDAC (Fig. 7I).

Discussion

In this study, we identify a fibroblast-intrinsic lipid signaling program that links CAF state to immune accessibility in PDAC. PTGDS was preferentially expressed in iCAFs and associated with increased T-cell infiltration and favorable clinical outcome. Functionally, increasing PTGDS expression in CAFs elevated PGD2 production, restrained tumor growth, and promoted $CD8^+$ T-cell accumulation, while exogenous PGD2 reproduced these effects and enhanced the antitumor activity of PD-1 blockade.

Mechanistically, PGD2 suppressed NF-κB activation and CCL2 production through its receptor DP2, and restoration of CCL2 reversed both the tumor-restraining and T-cell-permissive phenotypes associated with PTGDS-expressing CAFs. This functional relationship was further reproduced in a patient-matched system incorporating PDAC organoids, primary CAFs, and activated autologous PBMCs. Together, these findings define a PTGDS–PGD2–DP2–NF-κB/CCL2 axis through which fibroblast lipid signaling influences the immune organization of PDAC.

An important implication of these findings concerns the functional heterogeneity of CAFs in PDAC[29,30]. Although PTGDS was preferentially expressed in iCAFs, its expression was associated with increased T-cell infiltration, and enforced PTGDS expression in CAFs restrained tumor growth and promoted intratumoral $CD8^+$ T-cell accumulation.

These results demonstrate substantial functional heterogeneity within transcriptionally defined CAF subsets and establish PTGDS as a key immune-modulatory program specific to the iCAF compartment[16,31]. More broadly, our findings highlight the importance of resolving specific molecular programs within CAF populations when considering their contributions to the tumor immune microenvironment[24,32,33].

Our findings further extend CAF heterogeneity beyond canonical cytokine and extracellular matrix programs by identifying prostaglandin metabolism as a determinant of fibroblast immune function. Much of the work on fibroblast-mediated immune exclusion has focused on extracellular matrix organization, mechanical restriction, and protein mediators[34-36]. These mechanisms are clearly important; CAF-dependent matrix architecture can profoundly affect T-cell localization and function within solid tumors[34]. Our current data add a distinct metabolic layer to this framework. PTGDS expression increased PGD2 production by CAFs, and administration of PGD2 was sufficient to reproduce major features of the PTGDS-overexpression phenotype. These findings suggest that fibroblast metabolic state is not merely a consequence of CAF differentiation but can actively shape intercellular signaling within the tumor

microenvironment[16,17]. Locally generated lipid mediators may therefore provide a mechanism through which differences in fibroblast state are translated into broader changes in the immune landscape.

The biological effects of PGD2 are highly dependent on receptor identity and cellular context. PGD2 signals primarily through DP1 and DP2, which engage distinct downstream signaling programs[18-20]. In our CAF system, pharmacological inhibition of DP2 with AZD1981 substantially reversed PGD2-mediated suppression of p65 phosphorylation and CCL2 production, whereas inhibition of DP1 with asapiprant had little effect. These findings support DP2 as the receptor required for the PGD2 response observed in CAFs. This receptor dependence is consistent with emerging evidence that PGD2–PTGDR2 signaling can exert tumor-restraining effects in selected cancer contexts, although its biological consequences vary considerably across cell types and inflammatory states[19-21]. Importantly, our data do not yet define the complete biochemical cascade linking DP2 engagement to reduced NF-κB activity. Rather, they position DP2 upstream of the NF-κB–CCL2 module and provide a mechanistic framework for understanding how the enzymatic output of PTGDS is translated into an immune-regulatory CAF phenotype.

CCL2 emerged as a critical functional link between this lipid signaling program and the immune phenotype[23,25,27]. Transcriptomic profiling of PGD2-treated CAFs converged on cytokine and chemokine regulation, with CCL2 showing a prominent reduction at both the transcript and secreted-protein levels. Importantly, CCL2 supplementation reversed the suppression of tumor growth and the increase in $CD8^+$ T-cell infiltration produced by PTGDS-expressing CAFs in vivo. These rescue experiments distinguish CCL2 from a transcriptional correlate of PGD2 exposure and place its suppression functionally downstream of the PTGDS–PGD2 pathway.

The connection between PGD2 and CCL2 is further supported by our identification of NF-κB as an intervening signaling node. PGD2 reduced p65 phosphorylation without materially changing total p65 abundance, indicating regulation of NF-κB activation

rather than p65 expression. Pharmacological activation and inhibition of NF-κB produced corresponding changes in CCL2, while PGD2 attenuated LPS-induced p65 activation and CCL2 production. This relationship is particularly relevant in pancreatic fibroblasts, which are equipped to respond to tumor-derived inflammatory signals that activate NF-κB[14,15,28]. Our findings therefore suggest that PGD2–DP2 signaling functions as a counter-regulatory input within an inflammatory fibroblast state, limiting a component of its NF-κB-dependent chemokine output.

PGD2-mediated potentiation of the antitumor efficacy of PD-1 blockade carries potential therapeutic implications, although these findings should be interpreted in the context of our current experimental models. Immune checkpoint inhibition has shown limited activity in PDAC despite evidence that tumor-reactive T-cell responses can be induced or reinvigorated[5,37]. Immune checkpoint inhibition is unlikely to achieve efficacy in PDAC merely by restoring T cell effector function when T cells remain scarce within the tumor[38,39]. Our findings indicate that stromal signaling can modulate this upstream barrier of immune accessibility. PTGDS overexpression or PGD2 treatment increased intratumoral $CD8^+$ T-cell accumulation, and maximal tumor control was observed when these interventions were combined with PD-1 blockade. Recent studies similarly support the concept that manipulating the stromal or immune context can alter responsiveness to immunotherapy in PDAC [14,15,36]. These findings support a therapeutic concept in which modulation of stromal immune accessibility and checkpoint inhibition address complementary constraints on antitumor immunity[5,40]. Importantly, our experiments demonstrate enhanced activity of the combination rather than formal pharmacological synergy. Moreover, systemic manipulation of prostaglandin signaling may impact multiple immune and nonimmune compartments[19,38]. Translation of these findings will therefore require a clearer definition of the relevant cellular targets, receptor distribution, dose–response relationships, and consequences of sustained DP2 activation.

Several limitations define the boundaries of the present study. First, although single-

cell transcriptomics localized PTGDS predominantly to iCAFs and human tissue staining verified PTGDS expression in FAP^+ stromal cells, FAP is not an iCAF-specific marker. Thus, assignment of PTGDS to the iCAF state relies mainly on transcriptional annotation rather than direct spatial proof of PTGDS within molecularly defined iCAFs. Multiplex spatial profiling or RNA in situ hybridization combining PTGDS with validated iCAF markers would reinforce this conclusion and define the spatial localization of PTGDS-high fibroblasts relative to $CD8^+$ T cells and other TME components[9,30,41]. Second, the principal in vivo gain-of-function experiments used CAF–tumor cell co-implantation models. These models permit fibroblast-specific manipulation but do not fully reproduce the spatial organization, fibroblast ontogeny, and evolving immune microenvironment of spontaneous or orthotopic PDAC[9,26,31]. Fibroblast-restricted genetic manipulation of PtGDS in autochthonous models would provide a more stringent test of its endogenous function.

Third, our mechanistic evidence for DP2 is primarily pharmacological. The ability of AZD1981, but not asapiprant, to reverse PGD2-mediated suppression of NF-κB–CCL2 signaling strongly supports DP2 dependence; however, genetic deletion or silencing of *PTGDR2* in CAFs, followed by receptor rescue, would provide more definitive evidence of receptor specificity and exclude potential compound-specific off-target effects[19,20].

Fourth, although CCL2 supplementation establishes a functional role for CCL2 suppression in the PTGDS-associated phenotype, the downstream cellular targets of CCL2 remain incompletely resolved[23,25,27].

In summary, our study identifies PTGDS as an immune-regulatory program enriched in iCAFs and delineates a PTGDS–PGD2–DP2–NF-κB/CCL2 axis linking fibroblast lipid metabolism to the immune organization of PDAC. Instead of advocating nonselective fibroblast depletion, these findings highlight the value of dissecting distinct stromal functions[16,31,32]. Through CCL2 repression and enhanced $CD8^+$ T-cell accumulation, the PTGDS-PGD2–DP2 signaling axis remodels fibroblast compartments to create a microenvironment permissive to antitumor immunity and PD-

1 blockade. Collectively, these results imply that the therapeutic relevance of CAF heterogeneity extends beyond fibroblast subset ablation; the key lies in identifying and selectively modulating intra-fibroblast molecular programs that control immune exclusion[24,33].

Conflict of Interest

The authors declare no competing interests.

Authors' Contributions

Y. Liu: Conceptualization, data curation, investigation, methodology, validation, writing-original draft. Y. Ma: Data curation, investigation, methodology, writing-original draft. Y. Guo: Formal analysis, data curation, visualization. D. Tan: Investigation, methodology, data curation. H. Luo: data curation, visualization. W. Zhang: Investigation, resources. C. Zhang: visualization, validation. C. Shi: Conceptualization, funding acquisition, project administration, supervision, writing-review and editing.

Acknowledgments

This work was supported by the National Natural Science Foundation of China (32270566 and 32570629), Innovation Capability Support Program of Shaanxi (2025JC-GXPT-043 and 2024CX-GXPT-41), the Program of the State Key Laboratory of Holistic Integrative Management of Gastrointestinal Cancers (2025GTEP015).

Figure Legends

Figure 1. PTGDS is preferentially expressed in inflammatory CAFs and is associated with favorable clinical outcome in PDAC.

(A, B) PTGDS expression in pancreatic tumors and normal pancreatic tissues (A) and Kaplan–Meier overall survival analysis of patients stratified by PTGDS expression (B). (C–E) Integrated single-cell RNA-sequencing analysis of GSE231535 and GSE154778 showing the major cell populations (C), distribution of PTGDS expression (D), and PTGDS expression across annotated cell types (E). (F–I) Reclustering of the CAF compartment showing fibroblast clusters (F), annotation of seven CAF subtypes

(G), and the distribution of PTGDS expression across CAF populations (H, I). (J) Representative immunofluorescence images of human PDAC specimens stained for FAP (red), PTGDS (green), and DAPI (blue). Scale bar, 50 μm. Statistical significance is indicated in the corresponding panels.

Figure 1

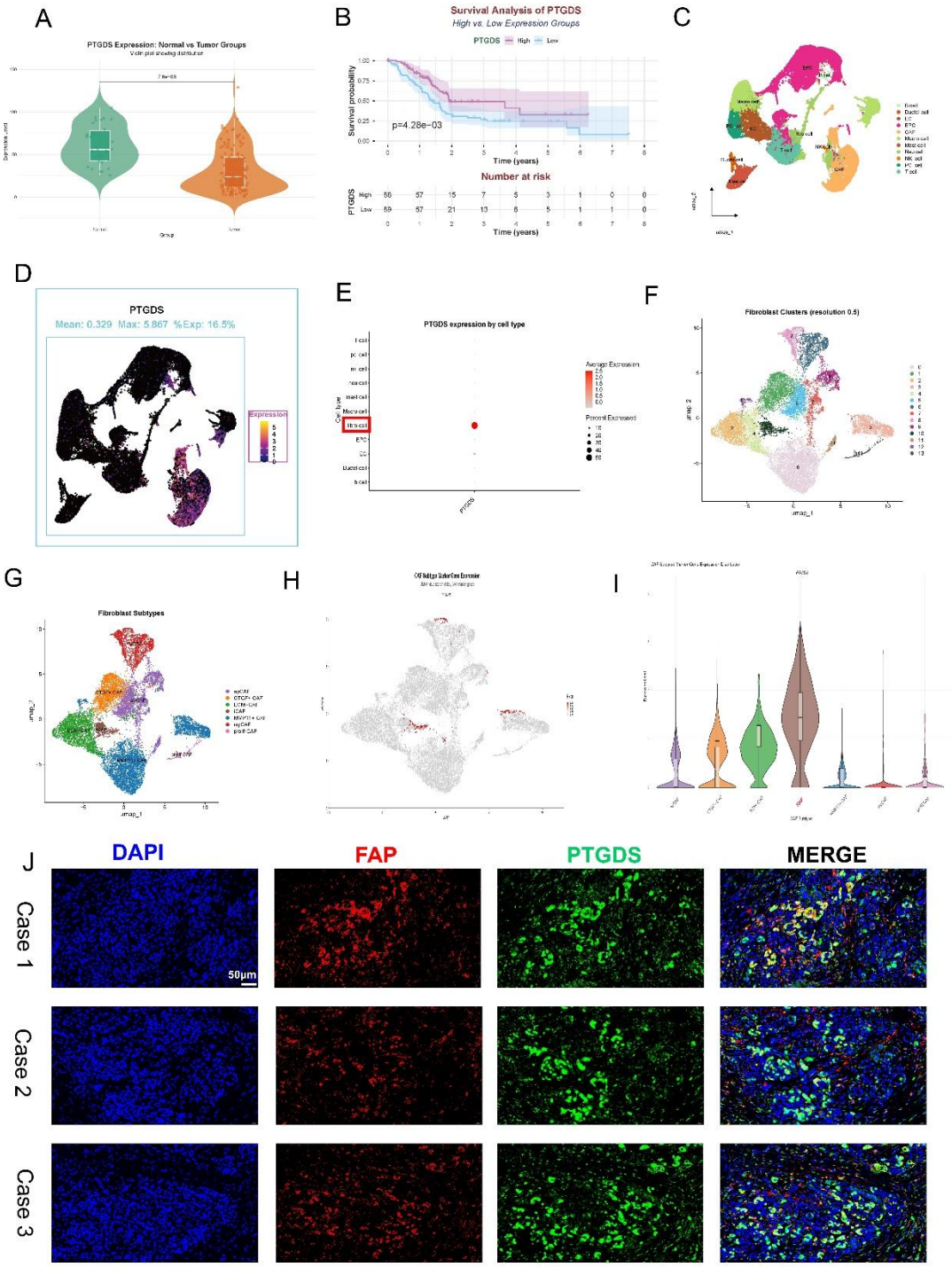

Figure 2. PTGDS expression is associated with a T-cell-infiltrated tumor microenvironment in PDAC.

(A) KEGG pathway enrichment analysis of PTGDS-associated genes. (B) Correlation

between PTGDS expression and inferred immune-cell abundance in PDAC. (C) Predicted cell–cell communication between CAF subpopulations and T cells based on single-cell transcriptomic analysis. (D) Correlation between PTGDS expression and the composite T-cell transcriptional score (Pearson r = 0.72, P = 0.0013). (E) Representative H&E and immunohistochemical staining for CD8 and PTGDS in human PDAC specimens with relatively low or high PTGDS expression. Scale bars, 50 μm.

Figure 2

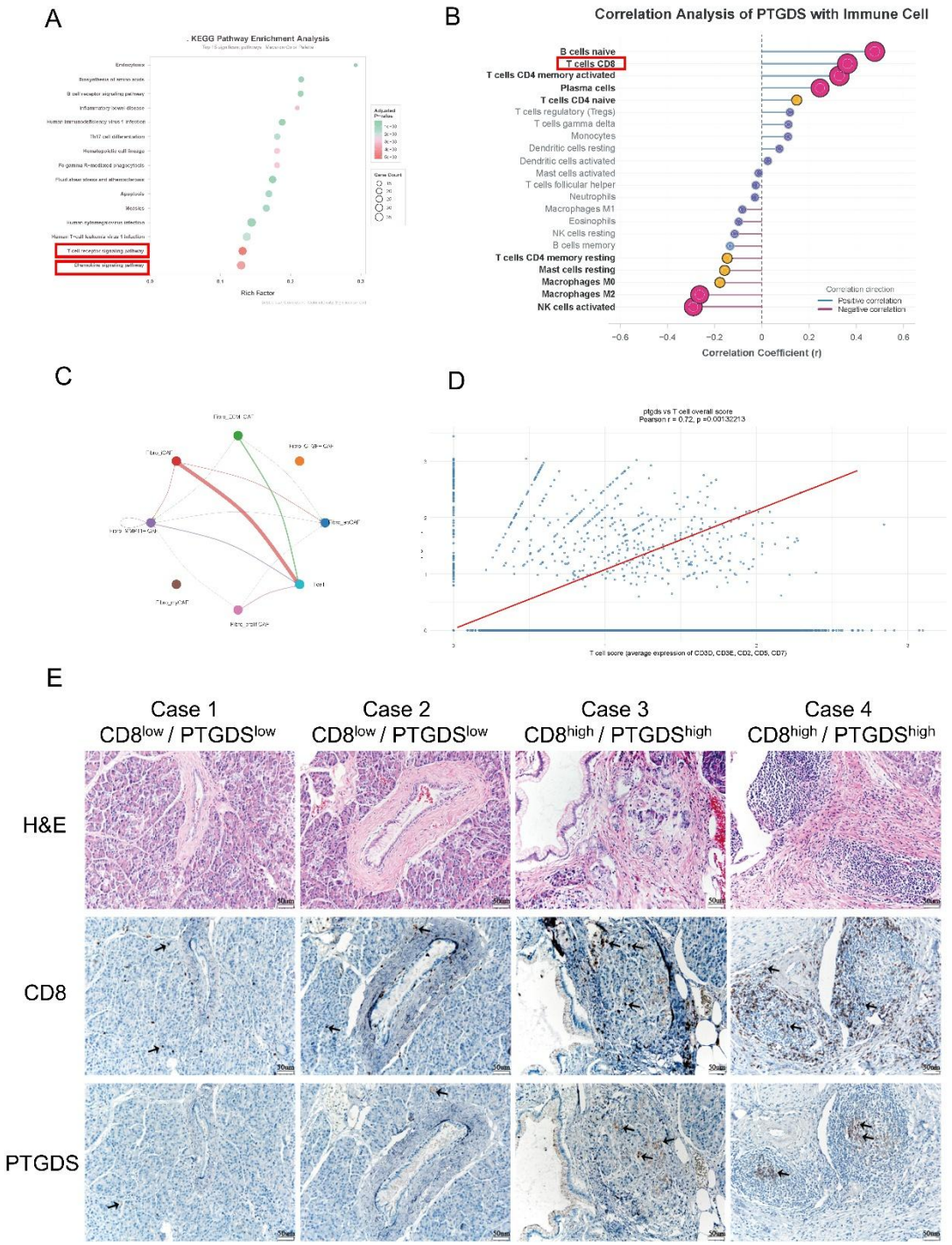

Figure 3. CAF-derived PTGDS restrains pancreatic tumor growth and enhances the antitumor activity of PD-1 blockade.

(A) Schematic of the CAF–tumor cell co-implantation model and treatment schedule.

KPC tumor cells were mixed with control (NC) or PTGDS-overexpressing (OE) KPC CAFs and subcutaneously implanted into C57BL/6J mice, followed by treatment with anti-PD-1 (α-PD-1) as indicated. (B–D) Representative images of excised tumors, tumor growth curves, and endpoint tumor weights in the NC, OE, NC + α-PD-1, and OE + α-PD-1 groups. (E, F) Representative immunohistochemical staining and corresponding quantification of Ki-67, CD8, GZMB, and PD-L1 in tumors from the indicated groups. Scale bars, 50 μm. Data are presented as mean ±SD (*n* = 6 mice per group).

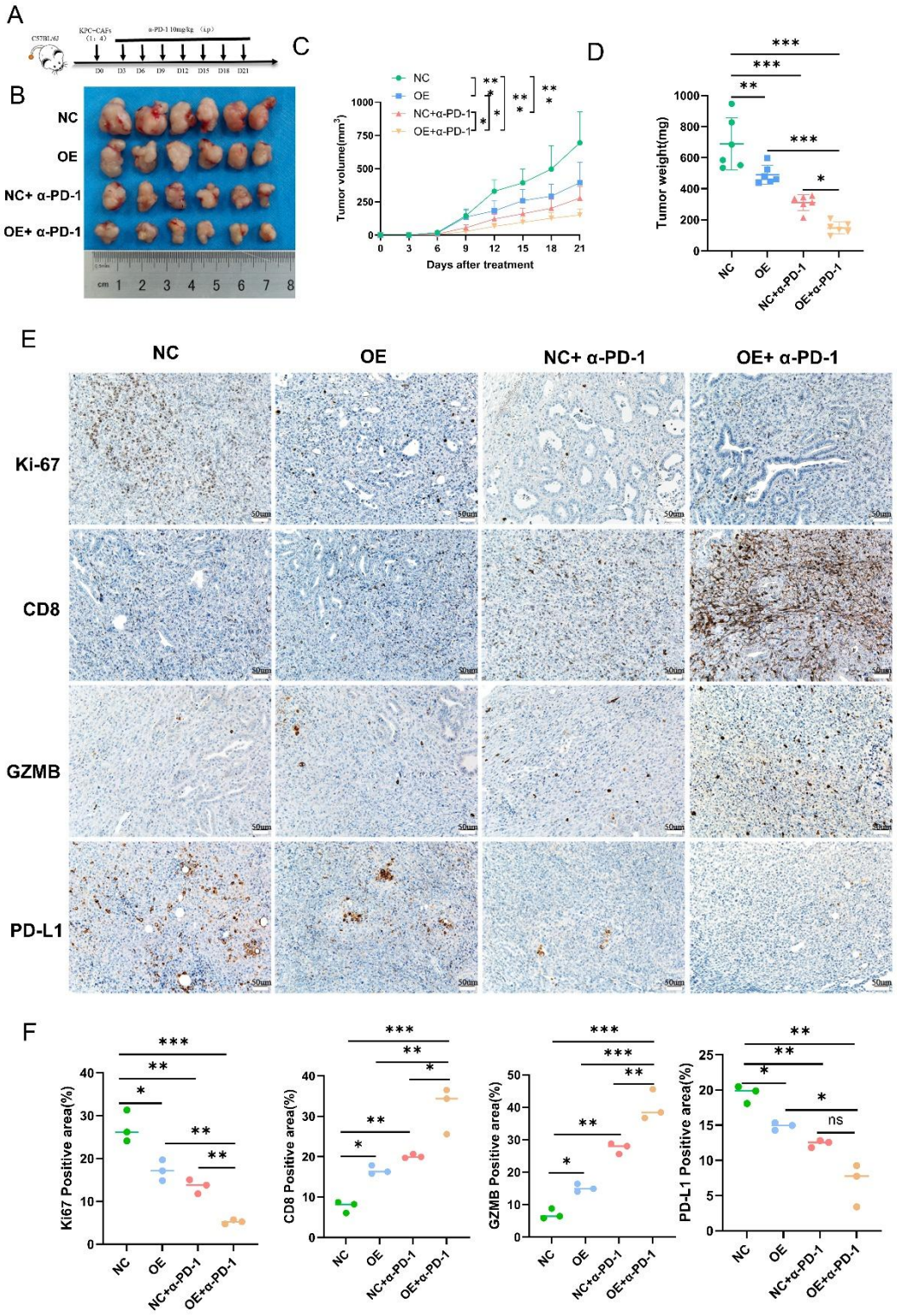

Figure 4. PGD2 mediates the tumor-restraining and immunomodulatory effects of CAF-derived PTGDS.

(A) PGD2-associated metabolic transcriptional activity in PTGDS-high and PTGDS-

low cells assessed using scMetabolism. (B, C) PGD2 levels in culture supernatants (B) and cell lysates (C) from control (NC) and PTGDS-overexpressing (OE) CAFs. (D–G) Schematic of the in vivo treatment protocol (D), representative images of excised tumors (E), tumor growth curves (F), and endpoint tumor weights (G) in mice treated with vehicle, PGD2, anti-PD-1 (α-PD-1), or PGD2 plus α-PD-1. (H) Representative immunohistochemical staining and corresponding quantification of Ki-67, CD8, GZMB, and PD-L1 in tumors from the indicated groups. Scale bars, 50 μm.

Figure 4

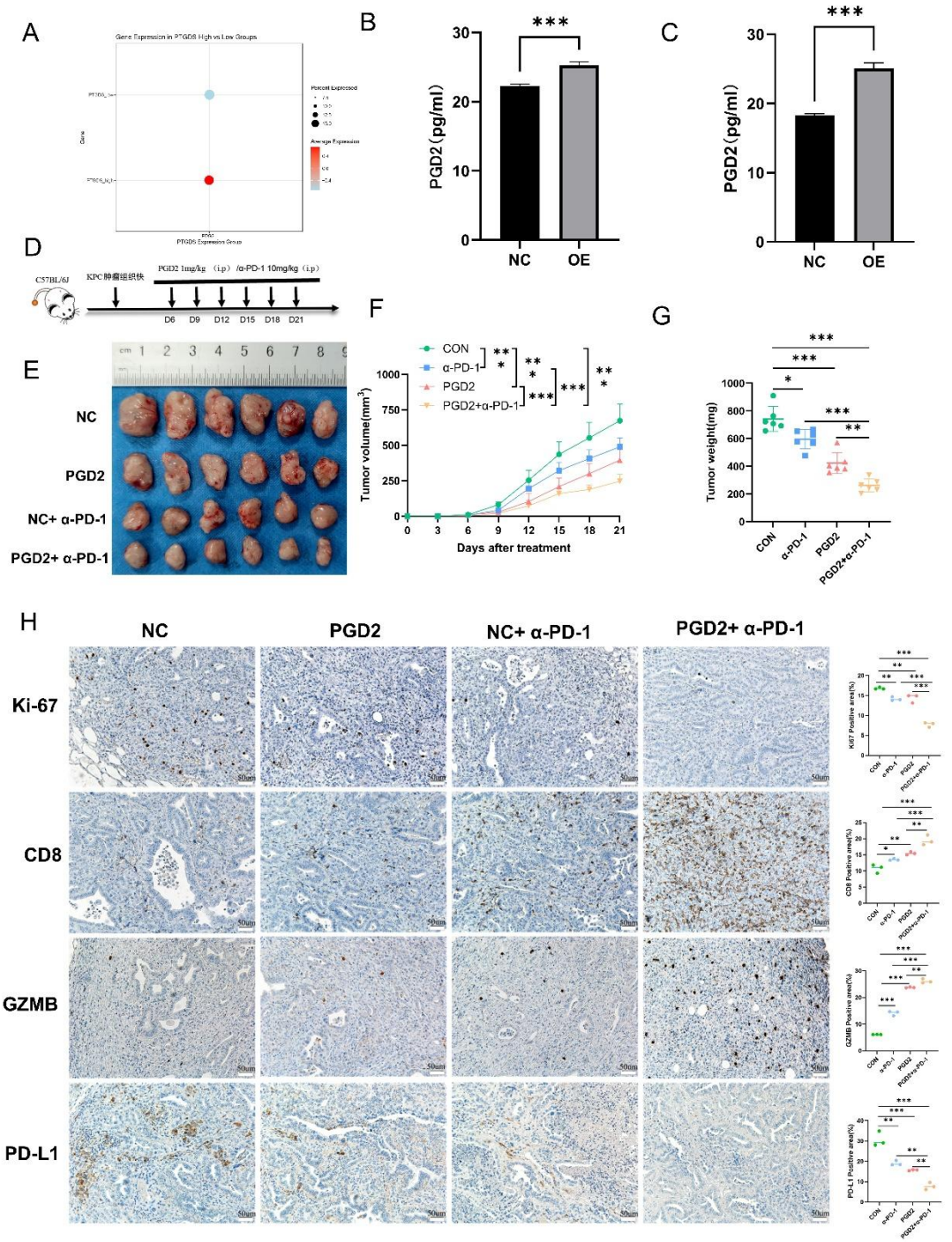

Figure 5. PGD2 suppresses CCL2 expression in CAFs.

(A, B) KEGG pathway enrichment analysis (A) and gene set enrichment analysis (GSEA) of cytokine–cytokine receptor interaction genes (B) following transcriptomic profiling of control and PGD2-treated CAFs. (C) Protein–protein interaction network of

PGD2-responsive genes, with CCL2 identified among the highly connected nodes. (D, E) qPCR analysis of the indicated cytokines and chemokines (D) and ELISA measurement of CCL2 in conditioned medium (E) from control and PGD2-treated CAFs. (F, G) Representative immunofluorescence staining for CCL2 (F) and corresponding quantification (G) in tumors from the vehicle, α-PD-1, PGD2, and PGD2 plus α-PD-1 groups. Scale bars, 50 μm.

Figure 5

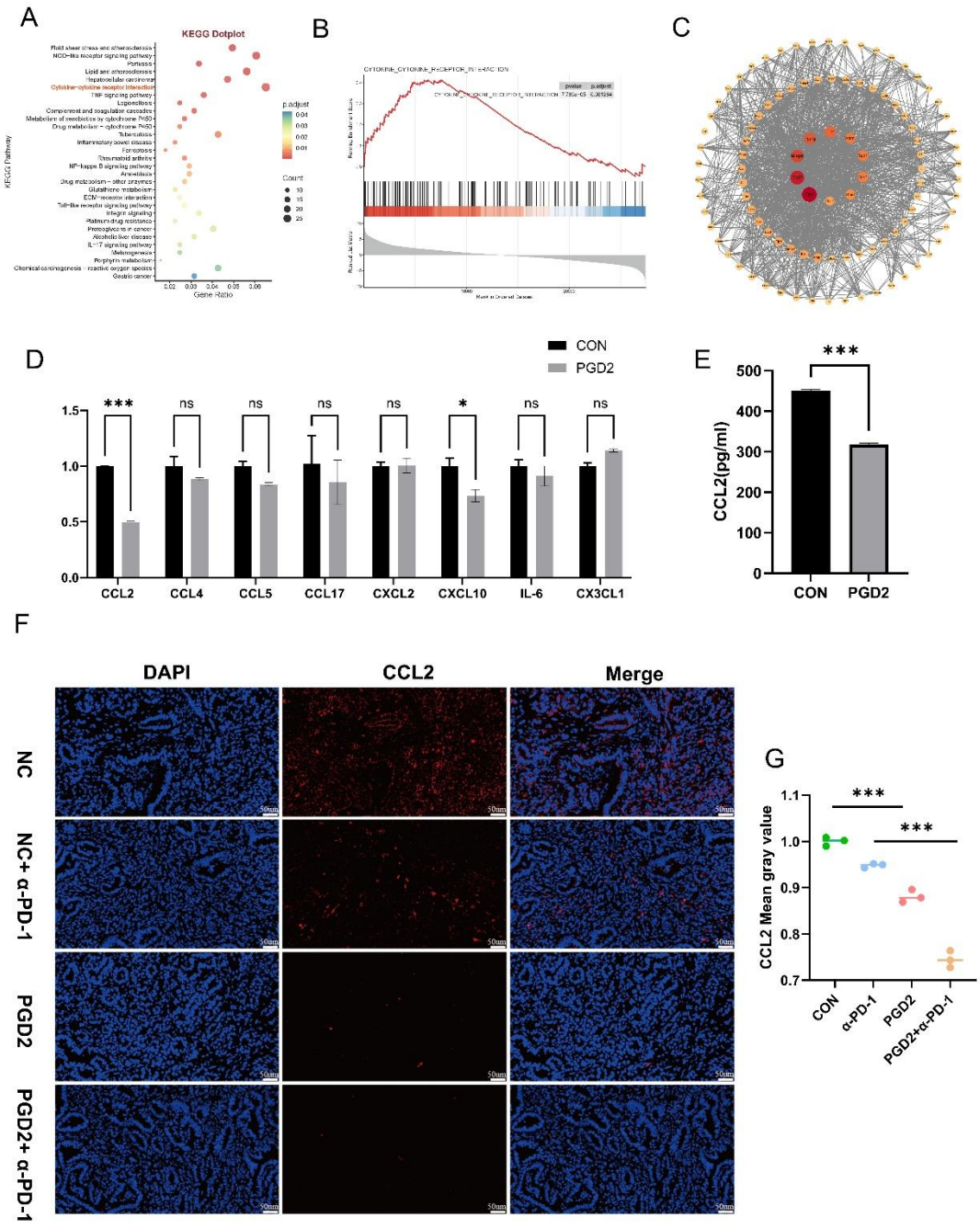

Figure 6. CCL2 suppression mediates the tumor-restraining and T-cell-permissive effects of CAF-derived PTGDS.

(A–D) Schematic of the in vivo CCL2 rescue experiment (A), representative excised

tumors (B), tumor growth curves (C), and endpoint tumor weights (D) in mice bearing KPC tumors containing control (NC) or PTGDS-overexpressing (OE) CAFs, with or without CCL2 supplementation. (E–G) Representative immunofluorescence staining for CD8 and CCL2 (E) and corresponding quantification of CD8 (F) and CCL2 (G) in tumors from the indicated groups. (H–J) Schematic of the patient-matched coculture system comprising patient-derived PDAC organoids (PDOs), primary CAFs, and activated autologous PBMCs (H), representative images of PDOs following coculture with control or PTGDS-overexpressing CAFs in the presence or absence of CCL2 supplementation (I), and corresponding quantification of PDO viability (J).

Figure 6

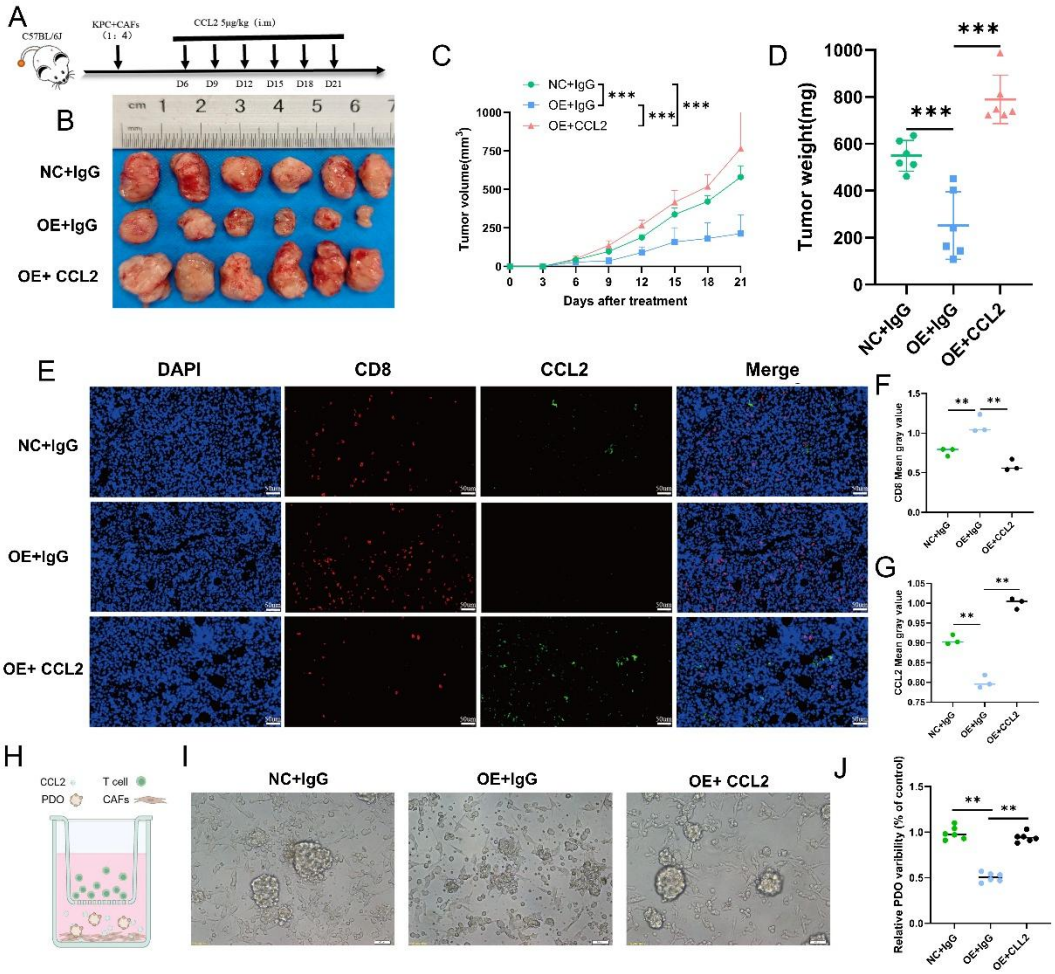

Figure 7. PGD2 suppresses NF-κB–CCL2 signaling in CAFs through DP2.

(A) GSEA of the NF-κB signaling pathway in transcriptomic profiles of control and PGD2-treated CAFs. (B) Immunoblot analysis of phosphorylated p65 (p-p65) and total p65 in CAFs following PGD2 treatment. (C–E) Immunoblot analysis of p-p65 and total p65 (C), CCL2 mRNA expression (D), and CCL2 secretion (E) in CAFs treated with PGD2, the NF-κB inhibitor BAY 11-7082, or LPS, alone or in combination as indicated. (F–H) Immunoblot analysis of p-p65 and total p65 (F), CCL2 mRNA expression (G), and CCL2 secretion (H) in PGD2-treated CAFs following pharmacological inhibition of DP1 with asapiprant or DP2 with AZD1981. GAPDH was used as the loading control. **(I)** Schematic illustration of the proposed mechanism by which the PTGDS–PGD2–DP2 axis suppresses NF-κB/CCL2 signaling in CAFs, thereby promoting $CD8^+$ T-cell infiltration, inhibiting PDAC tumor growth, and enhancing the efficacy of anti-PD-1 therapy.

Figure 7

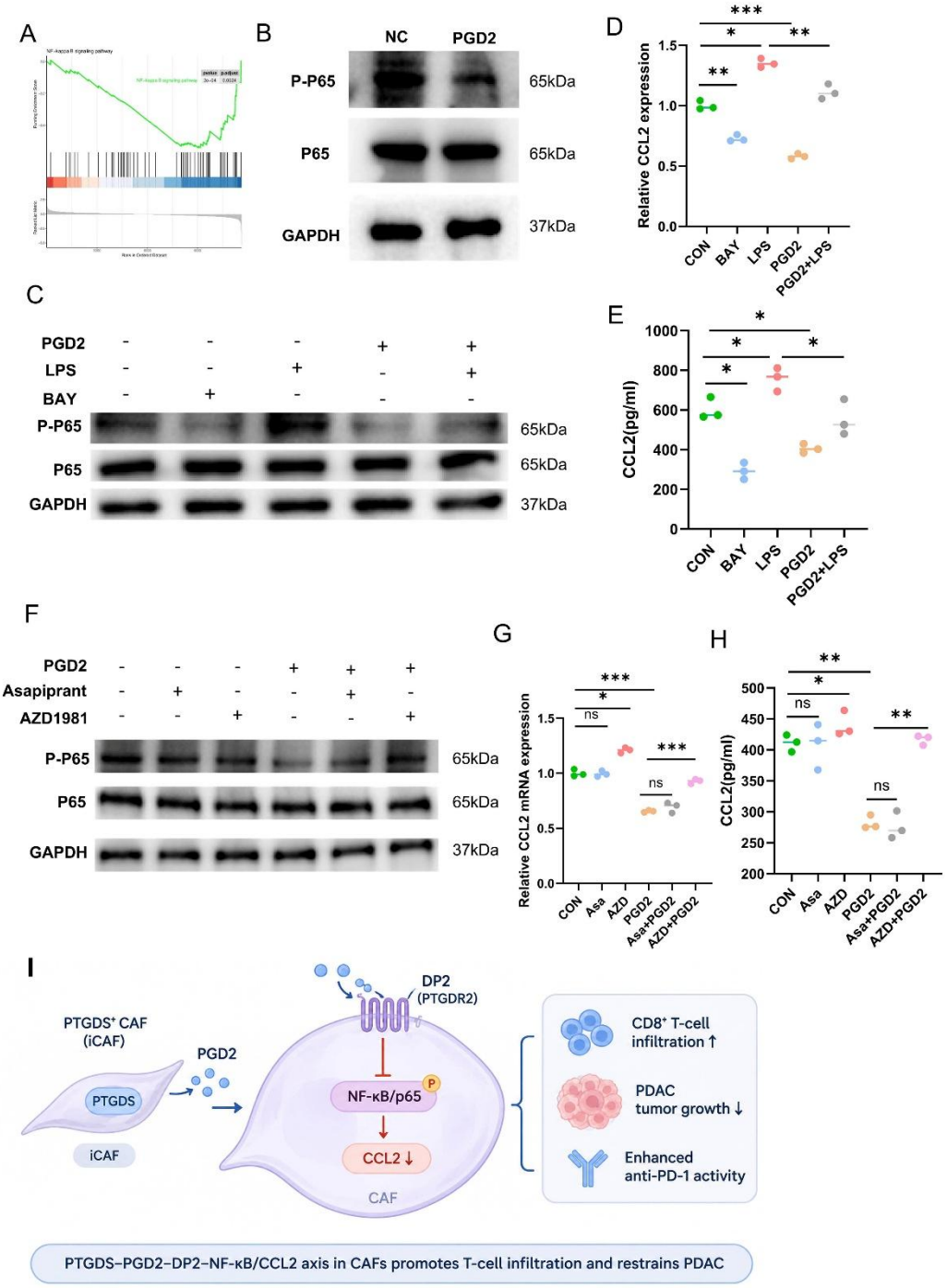

Supplementary Figure S1. Establishment of KPC-derived CAFs and validation of PTGDS overexpression.

(A–C) Schematic of the KPC mouse model (A), representative ultrasound imaging of a spontaneous pancreatic tumor (B), and H&E staining confirming pancreatic tumor formation (C). (D, E) Isolation and characterization of primary KPC-derived CAFs by

serial explant outgrowth (D) and FAP immunofluorescence staining (E). (F) Immunoblot validation of PTGDS overexpression in KPC CAFs. (G, H) Schematic of the CAF–T-cell coculture system (G) and flow-cytometric analysis of CD25 expression in T cells cocultured with control (NC) or PTGDS-overexpressing (OE) CAFs (H). Data are presented as mean ±SD from 3 independent experiments. $^{**}P < 0.05$. NC, negative control; OE, PTGDS overexpression.

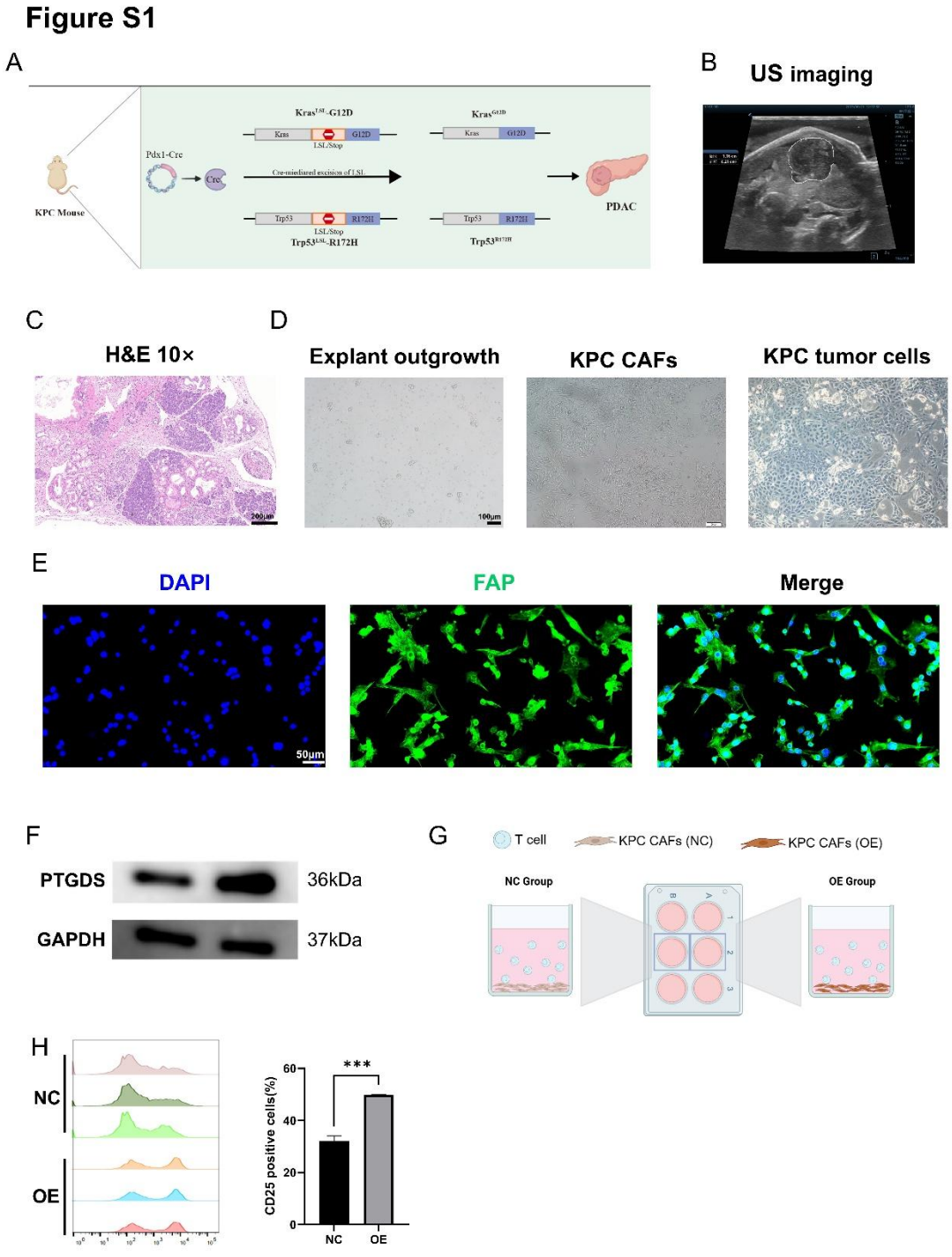

References

1 Siegel, R. L., Giaquinto, A. N. & Jemal, A. Cancer statistics, 2024. *CA Cancer J Clin* **74**, 12-49 (2024). https://doi.org/10.3322/caac.21820

2 Wainberg, Z. A. *et al.* NALIRIFOX versus nab-paclitaxel and gemcitabine in treatment-naive patients with metastatic pancreatic ductal adenocarcinoma (NAPOLI 3): a randomised, open-label, phase 3 trial. *Lancet* **402**, 1272-1281 (2023). https://doi.org/10.1016/s0140-6736(23)01366-1

3 Hwang, W. L. *et al.* Single-nucleus and spatial transcriptome profiling of pancreatic cancer identifies multicellular dynamics associated with neoadjuvant treatment. *Nat Genet* **54**, 1178-1191 (2022). https://doi.org/10.1038/s41588-022-01134-8

4 O'Reilly, E. M. *et al.* Durvalumab With or Without Tremelimumab for Patients With Metastatic Pancreatic Ductal Adenocarcinoma: A Phase 2 Randomized Clinical Trial. *JAMA Oncol* **5**, 1431-1438 (2019). https://doi.org/10.1001/jamaoncol.2019.1588

5 Padrón, L. J. *et al.* Sotigalimab and/or nivolumab with chemotherapy in first-line metastatic pancreatic cancer: clinical and immunologic analyses from the randomized phase 2 PRINCE trial. *Nat Med* **28**, 1167-1177 (2022). https://doi.org/10.1038/s41591-022-01829-9

6 Hernando-Calvo, A. *et al.* A Phase II, Open-Label, Randomized Trial of Durvalumab With Olaparib or Cediranib in Patients With Mismatch Repair-Proficient Colorectal or Pancreatic Cancer. *Clin Colorectal Cancer* **23**, 272-284.e279 (2024). https://doi.org/10.1016/j.clcc.2024.05.002

7 Kaplan, Z. *et al.* Clinical Implications of Mismatch Repair Deficiency in Pancreatic Ductal Adenocarcinoma. *Cancer Med* **14**, e70960 (2025). https://doi.org/10.1002/cam4.70960

8 Sherman, M. H. & Beatty, G. L. Tumor Microenvironment in Pancreatic Cancer Pathogenesis and Therapeutic Resistance. *Annu Rev Pathol* **18**, 123-148 (2023). https://doi.org/10.1146/annurev-pathmechdis-031621-024600

9 Helms, E. J. *et al.* Mesenchymal Lineage Heterogeneity Underlies Nonredundant Functions of Pancreatic Cancer-Associated Fibroblasts. *Cancer Discov* **12**, 484-501 (2022). https://doi.org/10.1158/2159-8290.Cd-21-0601

10 Ge, W. *et al.* PLA2G2A(+) cancer-associated fibroblasts mediate pancreatic cancer immune escape via impeding antitumor immune response of CD8(+) cytotoxic T cells. *Cancer Lett* **558**, 216095 (2023). https://doi.org/10.1016/j.canlet.2023.216095

11 Özdemir, B. C. *et al.* Depletion of carcinoma-associated fibroblasts and fibrosis induces immunosuppression and accelerates pancreas cancer with reduced survival. *Cancer Cell* **25**, 719-734 (2014). https://doi.org/10.1016/j.ccr.2014.04.005

12 Rhim, A. D. *et al.* Stromal elements act to restrain, rather than support, pancreatic ductal adenocarcinoma. *Cancer Cell* **25**, 735-747 (2014). https://doi.org/10.1016/j.ccr.2014.04.021

13 Elyada, E. *et al.* Cross-Species Single-Cell Analysis of Pancreatic Ductal

Adenocarcinoma Reveals Antigen-Presenting Cancer-Associated Fibroblasts. *Cancer Discov* **9**, 1102-1123 (2019). https://doi.org/10.1158/2159-8290.Cd-19-0094

14 Biffi, G. *et al.* IL1-Induced JAK/STAT Signaling Is Antagonized by TGFβ to Shape CAF Heterogeneity in Pancreatic Ductal Adenocarcinoma. *Cancer Discov* **9**, 282-301 (2019). https://doi.org/10.1158/2159-8290.Cd-18-0710

15 Sheng, N. *et al.* TAK1 Promotes an Immunosuppressive Tumor Microenvironment through Cancer-Associated Fibroblast Phenotypic Conversion in Pancreatic Ductal Adenocarcinoma. *Clin Cancer Res* **30**, 5138-5153 (2024). https://doi.org/10.1158/1078-0432.Ccr-24-1004

16 Niu, N. *et al.* Tumor cell-intrinsic epigenetic dysregulation shapes cancer-associated fibroblasts heterogeneity to metabolically support pancreatic cancer. *Cancer Cell* **42**, 869-884.e869 (2024). https://doi.org/10.1016/j.ccell.2024.03.005

17 Han, X. *et al.* Cancer-associated fibroblasts maintain critical pancreatic cancer cell lipid homeostasis in the tumor microenvironment. *Cell Rep* **43**, 114972 (2024). https://doi.org/10.1016/j.celrep.2024.114972

18 Islam, M. A., Khairnar, R., Fleishman, J., Thompson, K. & Kumar, S. Lipocalin-Type Prostaglandin D(2) Synthase Protein- A Central Player in Metabolism. *Pharm Res* **39**, 2951-2963 (2022). https://doi.org/10.1007/s11095-022-03329-4

19 Zhang, Q. *et al.* PGD2/PTGDR2 Signal Affects the Viability, Invasion, Apoptosis, and Stemness of Gastric Cancer Stem Cells and Prevents the Progression of Gastric Cancer. *Comb Chem High Throughput Screen* **27**, 933-946 (2024). https://doi.org/10.2174/1386207326666230731103112

20 Zhang, Q. *et al.* PGD2/PTGDR2 signaling pathway affects the self-renewal capacity of gastric cancer stem cells by regulating ATG4B ubiquitination. *Front Oncol* **14**, 1496050 (2024). https://doi.org/10.3389/fonc.2024.1496050

21 Li, J. *et al.* Pan cancer research reveals the role of PTGDS in tumor suppression and immune regulation. *NPJ Precis Oncol* **9**, 319 (2025). https://doi.org/10.1038/s41698-025-01097-z

22 Yan, R., Moresco, P., Gegenhuber, B. & Fearon, D. T. T cell-Mediated Development of Stromal Fibroblasts with an Immune-Enhancing Chemokine Profile. *Cancer Immunol Res* **11**, 1044–1054 (2023). https://doi.org/10.1158/2326-6066.Cir-22-0593

23 Bianchi, A. *et al.* Cell-Autonomous Cxcl1 Sustains Tolerogenic Circuitries and Stromal Inflammation via Neutrophil-Derived TNF in Pancreatic Cancer. *Cancer Discov* **13**, 1428-1453 (2023). https://doi.org/10.1158/2159-8290.Cd-22-1046

24 Belle, J. I. *et al.* Senescence Defines a Distinct Subset of Myofibroblasts That Orchestrates Immunosuppression in Pancreatic Cancer. *Cancer Discov* **14**, 1324-1355 (2024). https://doi.org/10.1158/2159-8290.Cd-23-0428

25 Li, X. *et al.* CCL2-mediated monocytes regulate immune checkpoint blockade resistance in pancreatic cancer. *Int Immunopharmacol* **106**, 108598 (2022). https://doi.org/10.1016/j.intimp.2022.108598

26 Gu, H., Deng, W., Zheng, Z., Wu, K. & Sun, F. CCL2 produced by pancreatic ductal adenocarcinoma is essential for the accumulation and activation of monocytic

myeloid-derived suppressor cells. *Immun Inflamm Dis* **9**, 1686-1695 (2021). https://doi.org/10.1002/iid3.523

27 Sanford, D. E. *et al.* Inflammatory monocyte mobilization decreases patient survival in pancreatic cancer: a role for targeting the CCL2/CCR2 axis. *Clin Cancer Res* **19**, 3404-3415 (2013). https://doi.org/10.1158/1078-0432.Ccr-13-0525

28 Fang, Z. *et al.* Signaling pathways in cancer-associated fibroblasts: recent advances and future perspectives. *Cancer Commun (Lond)* **43**, 3-41 (2023). https://doi.org/10.1002/cac2.12392

29 Zabransky, D. J. *et al.* Fibroblasts in the Aged Pancreas Drive Pancreatic Cancer Progression. *Cancer Res* **84**, 1221-1236 (2024). https://doi.org/10.1158/0008-5472.Can-24-0086

30 Dimitrieva, S. *et al.* Dynamic Evolution of Fibroblasts Revealed by Single-Cell RNA Sequencing of Human Pancreatic Cancer. *Cancer Res Commun* **4**, 3049-3066 (2024). https://doi.org/10.1158/2767-9764.Crc-23-0489

31 Carpenter, E. S. *et al.* Pancreatic Cancer-Associated Fibroblasts: Where Do We Go from Here? *Cancer Res* **84**, 3505-3508 (2024). https://doi.org/10.1158/0008-5472.Can-24-2860

32 Di Chiaro, P. *et al.* Mapping functional to morphological variation reveals the basis of regional extracellular matrix subversion and nerve invasion in pancreatic cancer. *Cancer Cell* **42**, 662-681.e610 (2024). https://doi.org/10.1016/j.ccell.2024.02.017

33 Oh, K. *et al.* Coordinated single-cell tumor microenvironment dynamics reinforce pancreatic cancer subtype. *Nat Commun* **14**, 5226 (2023). https://doi.org/10.1038/s41467-023-40895-6

34 Malchiodi, Z. X. *et al.* Periductal Fibroblast Density Defines Lymphocyte Exclusion via a CD44-Dependent Stromal Checkpoint in Pancreatic Cancer. *Cancer Immunol Res* (2026). https://doi.org/10.1158/2326-6066.Cir-25-1481

35 Xiao, Z. *et al.* Desmoplastic stroma restricts T cell extravasation and mediates immune exclusion and immunosuppression in solid tumors. *Nat Commun* **14**, 5110 (2023). https://doi.org/10.1038/s41467-023-40850-5

36 Kim, D. K. *et al.* PD-L1-directed PlGF/VEGF blockade synergizes with chemotherapy by targeting CD141(+) cancer-associated fibroblasts in pancreatic cancer. *Nat Commun* **13**, 6292 (2022). https://doi.org/10.1038/s41467-022-33991-6

37 Ali, L. R. *et al.* PD-1 Blockade Induces Reactivation of Nonproductive T-Cell Responses Characterized by NF-κB Signaling in Patients with Pancreatic Cancer. *Clin Cancer Res* **30**, 542-553 (2024). https://doi.org/10.1158/1078-0432.Ccr-23-1444

38 Hanahan, D., Michielin, O. & Pittet, M. J. Convergent inducers and effectors of T cell paralysis in the tumour microenvironment. *Nat Rev Cancer* **25**, 41-58 (2025). https://doi.org/10.1038/s41568-024-00761-z

39 Karamitopoulou, E. *et al.* Spatially restricted tumour-associated and host-associated immune drivers correlate with the recurrence sites of pancreatic cancer. *Gut* **72**, 1523-1533 (2023). https://doi.org/10.1136/gutjnl-2022-329371

40 Rojas, L. A. *et al.* Personalized RNA neoantigen vaccines stimulate T cells in

pancreatic cancer. *Nature* **618**, 144-150 (2023). https://doi.org/10.1038/s41586-023-06063-y

41 Grünwald, B. T. *et al.* Spatially confined sub-tumor microenvironments in pancreatic cancer. *Cell* **184**, 5577-5592.e5518 (2021). https://doi.org/10.1016/j.cell.2021.09.022